Letter

Joining microfluidics with infrared photodissociation: online-monitoring of isomeric flow-reaction intermediates

Maik Pahl, Martin Mayer, Maximilian Schneider, Detlev Belder, and Knut R. Asmis

Anal. Chem., **Just Accepted Manuscript** • DOI: 10.1021/acs.analchem.8b05532 • Publication Date (Web): 09 Jan 2019

Joining microfluidics with infrared photodissociation: online-monitoring of isomeric flow-reaction intermediates

Maik Pahl,[¥,£] Martin Mayer,[¢,£] Maximilian Schneider,[¥] Detlev Belder[¥,*] and Knut R. Asmis[¢,*]

[¥]Institut für Analytische Chemie, University Leipzig, Linnéstraße 3, 04103 Leipzig, Germany

[¢]Wilhelm-Ostwald-Institut für Physikalische und Theoretische Chemie, Universität Leipzig, Linnéstraße 2, 04103 Leipzig, Germany

[£]These authors contributed equally

ABSTRACT: A cryogenic ion trap vibrational spectrometer is combined with a microfluidic chip reactor in a proof-of-principle experiment on the Hantzsch cyclization reaction forming 2-amino-4-phenyl thiazole from phenacyl bromide and thiourea. First, the composition of the reaction solution is characterized using electrospray-ionization mass spectrometry combined with two-color infrared photodissociation (IRPD) spectroscopy. The latter yields isomer-specific vibrational spectra of the reaction intermediates and products. A comparison to results from electronic structure calculations then allows for an unambiguous structural assignment and molecular-level insights into the reaction mechanism. Subsequently, we demonstrate that isomeric and isobaric ions can be selectively monitored online with low process time, i.e. using a single IRPD wavelength per isomer, as the chip reaction parameters are varied.

The structural identification of reaction intermediates in solution is an essential aspect in unravelling reaction mechanisms and pathways in synthetic chemistry. The short lifetime of these transient species typically circumvents their proper analytical characterization. The advent of microfluidic technology in chemistry provided alternative approaches to shed new light on chemical processes at time and length scales hardly reachable with conventional technology.[1] When chemical conversions are performed in continuous flow microreactors[2-19] rather than in laboratory flasks, the reaction time coordinate is translated to the length scale of the reaction channel. By using short reaction channels and respective flow rates chemical conversions can be studied at minimum residence times far-from equilibrium. This opens up new routes to probe fast reactions in solution with minimal reagent consumption.[20-27]

For in-situ monitoring of chemical processes in microfluidic chips techniques such as fluorescence microscopy[28-31] or Raman microspectroscopy[32-34] are current state of the art. The coupling of microfluidic reactor chips with downstream mass spectrometry enables to probe the chemical constitution of reactor effluents.[35-37] Mass spectrometry, however, has limitations whenever isomeric compounds are present and there is currently a great demand for a technology for fast online monitoring of stereoselective processes at the microscale. For slower processes this can be achieved by on-chip integration of separation functionalities like electrophoresis or chromatography.[38-42]

An interesting candidate for on-the-fly structure-sensitive analysis is vibrational action spectroscopy by way of infrared photodissociation (IRPD).[43] IRPD allows for the isomer-specific monitoring of ions after they have been transferred into the gas phase, in particular, when this technique is combined with messenger-tagging[44-46] in cryogenic ion traps.[47-50] It's potential for characterizing solution phase reaction intermediates has recently been demonstrated.[51-59] Furthermore, IRPD spectroscopy combined with double–resonance laser excitation schemes in the form of double-resonance IR^2MS^2 spectroscopy[60-61] allows separating the spectroscopic signatures of isomeric and isobaric species in a general way (i.e. without the need of a UV/VIS chromophore as in ion dip spectroscopy[62]). This approach is highly complementary, for example, to recent combinations of IRPD spectroscopy with ion mobility measurements.[63-64]

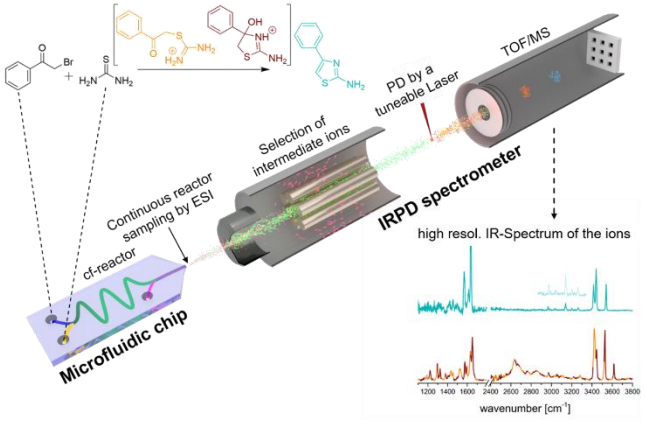

Figure 1. Schematic drawing of the microfluidic chip/IRPD spectrometer set-up. Reactants are mixed on chip. The reaction solution is continuously sampled using electrospray ionization in order to transfer ions into the gas phase, where they are characterized using vibrational action spectroscopy.

While IRPD spectroscopy gives access to high quality IR-spectra for unambiguous identification of gas-phase ions the rather high process times for recording a full spectrum have prevented its use for monitoring short-lived intermediates. In this contribution, we present a two-step approach to solve this challenge by joining microfluidics with IRPD. In this approach, reaction intermediates are first spectroscopically identified and subsequently the IRPD spectrometer is used to isomer-specifically monitor the chemical composition of a reactor effluent constantly spraying from a microfluidic chip (see Fig. 1).

Scheme 1: Mechanism of Hantzsch Cyclization Reaction

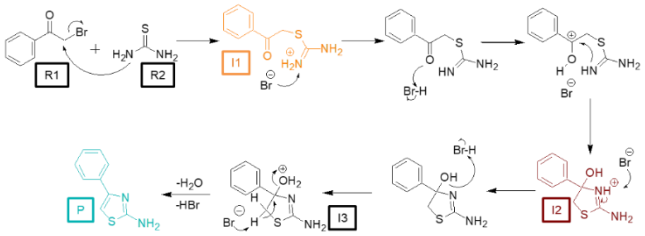

In order to characterize the properties and demonstrate the advantages of the chip-IRPD set-up, we apply the approach in a proof-of-concept study on the well-understood Hantzsch reaction shown in Scheme 1. This reaction is well suited as a litmus test for the approach in which the thiazole derivate **P** is formed from the reactants phenacyl bromide (**R1**) and thiuorea (**R2**) via three consecutively formed intermediates **I1-I3**. Note, all three intermediates **I1-I3** are isomers with the same m/z ratio of 195 amu. In order to characterize the structure and monitor the abundance of the reaction participants, in particular of the intermediates, we developed a tailored microfluidic chip (channel dimensions: 50 µm wide, 20 µm deep, 30 cm long, see supporting information for details) for this continuous flow reaction. The chip-device has an integrated electrospray emitter at its end to efficiently transfer the reaction solution into the high-vacuum chamber of the IRPD-triple mass spectrometer (Fig. S-3).

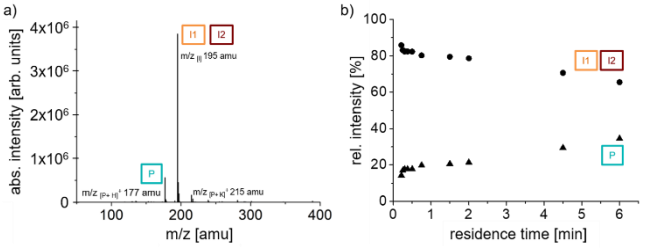

Figure 2. (a) ESI-MS spectrum of the continuous flow reaction using 2.5 mmol·L^{-1} phenacyl bromide and 1.0 mmol L^{-1} thiuorea in acetonitrile and flow rates corresponding to a chip residence time of 1 min. **(b)** Relative ion signal intensities of the protonated reaction product ([**P**+H]$^+$, m/z 177 amu, blue) and the intermediates (**I1** and **I2**, m/z 195 amu, orange and red) at residence times from 0.21 to 6.0 min. Relative ion signals are obtained by normalizing the mass spectrum intensities to the total ion yield.

First, we monitored the reaction yield as a function of the residence time of the reaction solution on the chip (see Fig. 2b). To this end, the reactant solutions, containing either **R1** or **R2**, are introduced into the first two inlets (see Fig. S-1) with an adjustable flow rate. A MeCN/H_2O solution (80:20, *v/v*) is supplied through a third inlet, at the end of the chip, to enhance the electrospray efficiency. The on-chip residence time is then determined from these flow rates and considering the chip geometry. A characteristic mass spectrum for a residence time of 1 min is show in Fig. 2a. Two dominant signals with m/z ratios of 177 amu and 195 amu, whose intensities change with varying residence time (see Fig. 2b), are detected. The signal at 177 amu corresponds to the protonated product [**P**+H]$^+$. Its relative intensity increases with longer residence times. The signal of the intermediates is found at 195 amu, which expectedly decreases with increasing residence and hence reaction time.

In a second step, we measured the vibrational spectrum of the product ion [**P**+H]$^+$. To this end, ions with m/z = 177 amu are mass-selected and subsequently trapped in a buffer-gas filled cryogenic ion trap held at 12 K. Here, the ions are thermalized close to the ambient temperature and messenger-tagged with D_2, which ensures measuring an IRPD spectrum in the linear absorption regime (see experimental section). The obtained IRPD spectrum in the spectral range from 1100 to 3800 cm^{-1} is shown in Fig. 3a. The spectrum reveals five characteristic IR bands, labeled a_1-a_5, a_7 and a_9 as well as some weaker signals. Comparison to the simulated IR spectrum of protonated 2-amino-4-phenylthiazole (see Fig. S-4 in the supporting information), obtained from density functional theory (DFT) calculations, which reproduces all the experimental spectrum satisfactorily, unambiguously identifies the structure of the [**P**+H]$^+$ ions and allows assigning these bands to individual vibrational modes (see Table S-1 for band assignments). Briefly, the intense absorptions above 3400 cm^{-1} (a_1-a_3) correspond to the N-H stretching modes of the primary and secondary amino groups. Band a_7 is the NH_2 bending mode and a_9 results from more delocalized modes involving C=C stretching and C-N-H bending motions.

Subsequently, we investigated the IR spectrum of the reaction intermediates, *i.e.* the ions with m/z = 195 amu. The obtained IRPD spectrum in the O-H and N-H stretching region is shown in the bottom panel of Fig. 3b. Similar to the spectrum of the product ion [**P**+H]$^+$, it can be assigned based on a comparison to simulated IR spectra of the three possible reaction intermediates **I1** to **I3** (see Fig. S-5 and Table S-2 for band assignments). The assignment of the experimental spectrum (Fig. 3b) is straightforward. Contributions from **I3**, which contains the water adduct and hence is characterized by two characteristic O-H stretching modes in the region above 3600 cm^{-1}, can be excluded, since only a single band is observed at 3618 cm^{-1} (b_1) in the experimental spectrum. Moreover, intermediate **I1** does not contain an O-H group and so **I2** must be present to account for band b_1. Indeed, the predicted IR spectrum of **I2** (Fig. S-5b) shows a satisfactory agreement with the experimental one. However, the experimental spectrum reveals additional bands, in particular b_6, which can only be rationalized assuming the coexistence of **I2** and **I1.** Assuming the presence of both of these intermediates with a 1:1 ratio results in the best agreement with the experimental spectrum (see Fig. S-5d).

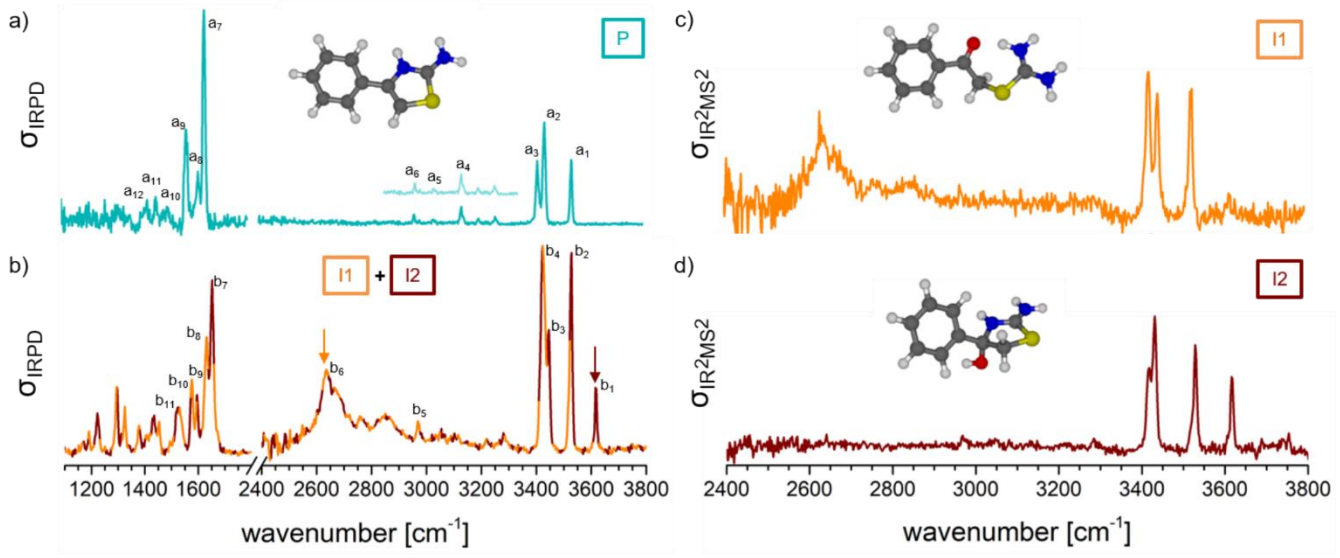

Figure 3. (**a**) IRPD spectrum of D_2-tagged [**P**+H]$^+$ ions (blue). (**b**) The experimental spectrum of the ions **I1** (orange) and **I2** (red) corresponding to the signal at m/z = 195 amu in Fig. 2. **P, I1** and **I2** are formed in the chip reaction, transferred in their protonated form by ESI to the high vacuum chamber and their IR spectra are subsequently measured using IRPD. The corresponding minimum energy structure (H: white, C: grey, N: blue, S: yellow, O: red) is also shown. Simulated IR spectrum of D_2-tagged ions (Fig. S-4, S-5) and band assignments (Tab. S-1, S-2) are shown in supporting information. (**c,d**) Isomer-specific IR^2MS^2 spectra of **I1** (**c**, orange), and **I2** (**d**, red) in the range between 2400 and 3800 cm^{-1}, confirming the presence of two stable intermediates. The spectra of **I1** and **I2** were obtained by pumping their isomer-specific modes at 2636 cm^{-1} and 3618 cm^{-1}, respectively.

In order to confirm the presence of both intermediates and reveal their individual IR signatures, we performed isomer-specific IR^2MS^2 measurements in the range between 2400 and 3800 cm^{-1} and these are shown in Figs. 3c-d. Briefly, this double-resonance method allows measuring the IRPD spectra of coexisting isomers, whenever the IR spectra of the corresponding isomers differ significantly at least at one wavelength. In the present case, we obtained the IR^2MS^2 spectrum of **I1** (Fig. 3c) by pumping the isomer-specific NH stretching mode b_6 and that of **I2** (Fig. 3d) by pumping the isomer-specific O-H stretching mode b_1. The two IR^2MS^2 spectra convincingly show that these two, and only these two, constitutional isomers are responsible for the ion signal at m/z = 195 amu.

A major advantage of the microfluidic setup is that the conditions on the chip can be changed quickly. In combination with the IRPD detection scheme it is then possible to monitor the influence of these changes online and obtain isomer-resolved kinetic information. Note, this does not require to measure complete IRPD spectra over broad spectral ranges, which indeed would be very time consuming. Once the IR spectra of the individual reaction participants have been disentangled using the IR^2MS^2 scheme, isomer-specific ion signals can be obtained, in the best case, by probing at a single wavelength per isomer and the resulting ion signals can then be converted to ion yields based on calibration tables. Such a procedure, in principle, takes only 100 ms, given the 10 Hz repetition rate of the photodissociation laser. However, fluctuations of the laser pulse energy as well as of the ion signal require to typically average over at least 10 to 20 laser shots in order to obtained a satisfactory signal-to-noise ratio.

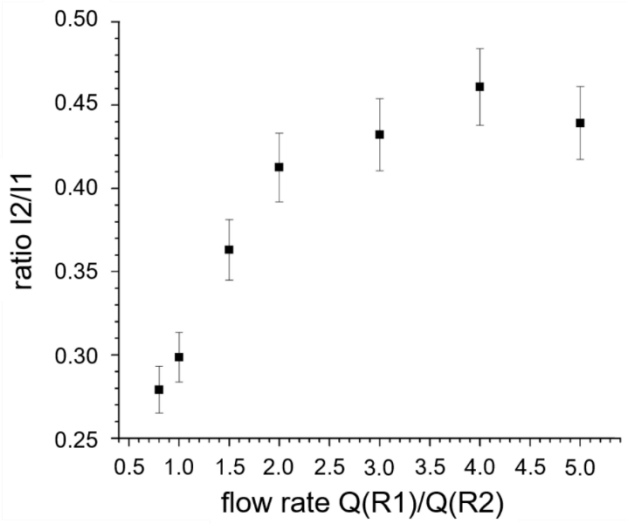

Figure 4. The ratio of **I2/I1** as a function of the reactant solution flow ratio Q(**R1**)/Q(**R2**) measured by monitoring the ion yield of the intermediates **I1** and **I2** spectroscopically at 3445 cm^{-1} and 3618 cm^{-1}, respectively.

To demonstrate the analytical possibilities of this approach we determined the optimal flow rate ratio of the reactant solutions with respect to the highest product yield by monitoring the relative intermediate ratio **I2/I1** (see Fig. 4) using this technique. The fastest possible reaction is obtained when this yield is maximized. The ion yields were determined by monitoring the ion signals of the intermediates **I1** and **I2** by probing at 3445 cm^{-1} (**I1**) and 3618 cm^{-1} (**I2**), while systematically changing the flow rate of the individual reactant solutions containing **R1** and **R2**. The initial concentrations, 2.5 mmol·L^{-1} phenacyl bromide and 1.0 mmol L^{-1}

thiuorea, of both reactants and the total flow rate (1.2 µL min^{-1}, residence time: 25 s) were kept unchanged.

The data in Fig. 4 shows that a flow rate ratio of one, i.e. equal flow rates for both solutions is far from optimal. A maximum in the **I2/I1** ratio, indicating the reaction that has proceeded the farthest, is obtained for a flow rate ratio of around 4.0. Even though the conversion of flow rates to local concentrations is not straight forward, the present results suggest that the transformation of **R1** is involved in the rate-limiting step of the reaction and therefore needs to be present in excess. This is in agreement assuming a S_N1 type reaction, which exhibits a first order dependence on the concentration of the electrophile (**R1**) and a zeroth-order dependence on the concentration of the nucleophile (**R2**). Similar results were obtained, when the initial concentrations of the reactants were changed.

In summary, we have demonstrated that IRPD combined with lab-on-a-chip technology allows to identify, characterize and monitor reactants, products and short-lived intermediates of continuous flow reactions. Vibrational spectra of the corresponding gas phase ions can be measured over a broad spectral region, allowing for an unambiguous structural assignment based on a comparison to simulated spectra from electronic structure calculations. After a characteristic wavelength has been determined for each reaction participant, their abundance can be monitored isomer-specifically on a time scale of seconds or less as the on-chip reaction parameters are optimized. Hence, the present technique represents a powerful new addition to the lab-on-a-chip tool kit for studying reaction kinetics and unraveling reaction mechanisms of continuous flow reactions.

ASSOCIATED CONTENT

Supporting Information

The Supporting Information is available free of charge on the ACS Publications website.
Detailed description of the microfluidic fabrication process; picture of the experimental setup; mechanism of the Hantzsch reaction; MS spectrum of the Chip-MS-IRPD measurement; Chip-MS spectrum of the changes conditions (PDF).

AUTHOR INFORMATION

Corresponding Author

© Phone: +49 341 97 36421; Fax: +49 341 97 36399; E-mail: knut.asmis@uni-leipzig.de
¥ Phone: +49 341 97 36091; Fax: +49 341 97 36115; E-mail: belder@uni-leipzig.de

Notes

The authors declare no competing financial interest.

ACKNOWLEDGMENT

Financial support by the German Research Foundation (DFG, FOR 2177) is gratefully acknowledged. K.R.A. acknowledges instrumental support from the Fritz-Haber-Institute of the Max-Planck Society.

REFERENCES

1 deMello, A. J.; Control and detection of chemical reactions in microfluidic systems, *Nature* **2006**, *442*, 394–402.
2 Webb, D.; Jamison, T. F.; Continuous flow multi-step organic synthesis, *Chem. Sci.* **2010**, *1*, 675–680.
3 Wegner, J.; Ceylan, S.; Kirschning, A.; Flow Chemistry – A Key Enabling Technology for (Multistep) Organic Synthesis, *Adv. Synth. Catal.* **2012**, *354*, 17–57.
4 Jas, G.; Kirschning, A.; Continuous Flow Techniques in Organic Synthesis, *Chem. Eur. J.* **2003**, *9*, 5708–5723.
5 Myers, R. M.; Fitzpatrick, D. E.; Turner, R. M.; Ley, S. V.; Flow Chemistry Meets Advanced Functional Materials, *Chem. Eur. J.* **2014**, *20*, 12348–12366.
6 Knowles, J. P.; Elliott, L. D.; Booker-Milburn, K. I.; Flow photochemistry: Old light through new windows, *Beilstein J. Org. Chem.* **2012**, *8*, 2025–2052.
7 Wiles, C.; Watts, P.; Continuous process technology: a tool for sustainable production, *Green Chem.* **2014**, *16*, 55–62.
8 Vaccaro, L.; Lanari, D.; Marrocchia, A.; Strappaveccia, G.; Flow approaches towards sustainability, *Green Chem.* **2014**, *16*, 3680–3704.
9 Wegner, J.; Ceylan, S.; Kirschning, A.; Flow Chemistry – A Key Enabling Technology for (Multistep) Organic Synthesis, *Adv. Synth. Catal.* **2012**, *354*, 17–57.
10 Protasova, L. N.; Bulut, M.; Ormerod, D.; Buekenhoudt, A.; Berton, J.; Stevens, C. V.; Latest Highlights in Liquid-Phase Reactions for Organic Synthesis in Microreactors, *Org. Process Res. Dev.* **2013**, *17*, 760–791.
11 Noël, T.; Buchwald, S. L.; Cross-coupling in flow, *Chem. Soc. Rev.* **2011**, *40*, 5010–5029.
12 Baxendale, I. R.; The integration of flow reactors into synthetic organic chemistry, *J. Chem. Technol. Biotechnol* **2013**, *88*, 519–552.
13 McQuade, D. T.; Seeberger, P. H.; Applying Flow Chemistry: Methods, Materials, and Multistep Synthesis, *J. Org. Chem.* **2013**, *78*, 6384–6389.
14 Hartman, R. L.; Jensen, K. F.; Microchemical systems for continuous-flow synthesis, *Lab Chip* **2009**, *9*, 2495–2507.
15 Webb, D.; Jamison, T. F.; Continuous flow multi-step organic synthesis, *Chem. Sci.* **2010**, *1*, 675–680.
16 Bédard, A.; Adamo, A.; Aroh, K. C.; Russell, M. C.; Bedermann A. A.; Torosian, J.; Yue, B., Jensen, K. F. Jamison, T. F.; Reconfigurable system for automated optimization of diverse chemical reactions, *Science* **2018**, *361*, 1220–1225.
17 Jensen, K. F.; Flow chemistry – Microreaction technology comes of age, *AIChE J.* **2017**, *63*, 858–867.
18 Adamo, A.; Beingessner, R.L.; Behnam, M.; Chen, J.; Jamison, T.F.; Jensen, K.F.; Monbaliu, J.-C. M.; Myerson, A.S.; Revalor, E.M.; Snead, D.R.; Stelzer, T.; Weeranoppanant, N.; Wong, S.Y.; Zhang P.; On-demand continuous-flow production of pharmaceuticals in a compact, reconfigurable system, *Science* **2016**, *352*, 61–67.
19 Fitzpatrick, D.E.; Battilocchio, C.; Ley S.V.; Enabling Technologies for the Future of Chemical Synthesis, *ACS Cent. Sci.* **2016**, *2*, 131–138.
20 Sorrenti, A.; Rodriguez-Trujillo, R.; Amabilino, D.B.; Puigmartí-Luis, J.; Milliseconds Make the Difference in the Far-from-Equilibrium Self-Assembly of Supramolecular Chiral Nanostructures, *J. Am. Chem. Soc.* **2016**, *138*, 6920–6923.
21 Knight, J. B.; Vishwanath, A.; Brody, J. P.; Austin, R. H.; Hydrodynamic Focusing on a Silicon Chip: Mixing Nanoliters in Microseconds, *Phys. Rev. Lett.* **1998**, *80*, 3863–3866.
22 Shastry, M. C. R.; Luck, S. D.; Roder, H. A.; A Continuous-Flow Capillary Mixing Method to Monitor Reactions on the Microsecond Time Scale, *Biophys. J.* **1998**, *74*, 2714–2721.

23 Mitchell, M. C.; Spikmans, V.; de Mello, A. J.; Microchip-based synthesis and analysis: Control of multicomponent reaction products and intermediates, *Analyst* **2001**, *126*, 24–27.

24 Yan, X; Cheng, H.; Zare, R. N.; Two-Phase Reactions in Microdroplets without the Use of Phase-Transfer Catalysts, *Angew. Chem. Int. Ed.* **2017**, *56*, 3562–3565.

25 Banerjee, S.; Zare, R. N.; Syntheses of Isoquinoline and Substituted Quinolines in Charged Microdroplets, *Angew. Chem. Int. Ed.* **2015**, *54*, 14795–14799.

26 Girod, M.; Moyano, E.; Campbell, D. I.; Cooks, R. G.; Accelerated bimolecular reactions in microdroplets studied by desorption electrospray ionization mass spectrometry, *Chem. Sci.* **2011**, *2*, 501–510.

27 Nowbahar, A.; Mansard, V.; Mecca, J. M.; Paul, M.; Arrowood, T.; Squires, T. M.; Measuring Interfacial Polymerization Kinetics Using Microfluidic Interferometry, *J. Am. Chem. Soc.* **2018**, *140*, 3173–3176.

28 Kauffmann, E.; Darnton, N. C.; Austin, R.H.; Batt C.; Gerwert, K.; Lifetimes of intermediates in the β-sheet to α-helix transition of β-lactoglobulin by using a diffusional IR mixer, *Proc. Natl. Acad. Sci. U S A.* **2001**, *98*, 6646–6649.

29 Maceiczyk, R. M.; Dümbgen, K.; Lignos, I.; Protesescu, L.; Kovalenko, M. V.; de Mello, A. J.; Microfluidic Reactors Provide Preparative and Mechanistic Insights into the Synthesis of Formamidinium Lead Halide Perovskite Nanocrystals, *Chem. Mater.* **2017**, *29*, 8433–8439.

30 Lipman, E. A.; Schuler, B.; Bakajin, O.; Eaton, W. A.; Single-Molecule Measurement of Protein Folding Kinetics, *Science* **2003**, *30*, 1233–1235.

31 Dingfelder, F.; Wunderlich, B.; Benke, S.; Zosel, F.; Zijlstra, N.; Nettels, D.; Schuler, B.; Rapid Microfluidic Double-Jump Mixing Device for Single-Molecule Spectroscopy, *J. Am. Chem. Soc.* **2017**, *139*, 6062–6065.

32 Xie, W.; Grzeschik, R.; Schlücker, S.; Metal Nanoparticle-Catalyzed Reduction Using Borohydride in Aqueous Media: A Kinetic Analysis of the Surface Reaction by Microfluidic SERS, *Angew. Chem. Int. Ed.* **2016**, *55*, 13729–13733.

33 Meier, T. A.; Beulig, R. J.; Klinge, E.; Fuss, M.; Ohla, S.; Belder, D.; On-chip monitoring of chemical syntheses in microdroplets via surface-enhanced Raman spectroscopy, *Chem. Commun.* **2015**, *51*, 8588–8591.

34 Zhang, Z.; Gernert, U.; Gerhardt, R.; Höhn, E.-M., Belder, D. Kneipp, J.; Catalysis by Metal Nanoparticles in a Plug-In Optofluidic Platform: Redox Reactions of *p*-Nitrobenzenethiol and *p*-Aminothiophenol, *ACS Catal.* **2018**, *8*, 2443–2449.

35 Mitchell, M. C., Spikmans, V, de Mello, A. J.; Microchip-based synthesis and analysis: Control of multicomponent reaction products and intermediates, *Analyst.* **2001**, *126*, 24–7.

36 Dietze, C.; Schulze, S.; Ohla, S.; Gilmore, K.; Seeberger, P. H.; Belder, D.; Integrated on-chip mass spectrometry reaction monitoring in microfluidic devices containing porous polymer monolithic columns, *Analyst* **2016**, *141*, 5412–5416.

37 Appun, J.; Boomhoff, M.; Hoffmeyer, P.; Kallweit, I.; Pahl, M.; Belder, D.; Schneider, C.; A Highly Stereoselective Synthesis of Tetrahydrofurans, *Angew. Chem. Int. Ed.* **2017**, *24*, 6758–6761.

38 Warias, R.; Zaghi, A.; Heiland, J. J.; Piendl, S. K.; Gilmore, K.; Seeberger, P. H.; Massi, A.; Belder, D.; An Integrated Lab-on-a-chip Approach to Study Heterogeneous Enantioselective Catalysts at the Microscale, *ChemCatChem* **2018**, *10*, 5382–5385.

39 Heiland, J. J.; Warias, R.; Lotter, C.; Fuchs, P.; Mauritz, L.; Zeitler, K.; Ohla, S.; Belder, D.; On-chip integration of organic synthesis and HPLC/MS analysis for monitoring stereoselective transformations at the micro-scale, *Lab Chip* **2017**, *17*, 76–81.

40 Lotter, C.; Poehler, E.; Heiland, J. J.; Mauritz, L.; Belder, D.; Enantioselective reaction monitoring utilizing two-dimensional heart-cut liquid chromatography on an integrated microfluidic chip, *Lab Chip* **2016**, *16*, 4648–4652.

41 Krone, K. M.; Warias, R.; Ritter, C.; Li, A.; Acevedo-Rocha, C. G.; Reetz, M. T.; Belder, D.; Analysis of Enantioselective Biotransformations Using a Few Hundred Cells on an Integrated Microfluidic Chip, *J. Am. Chem. Soc.* **2016**, *138*, 2102–2105.

42 Fritzsche, S.; Ohla, S.; Glaser, P.; Giera, D. S.; Sickert, M.; Schneider, C.; Belder, D.; Asymmetric Organocatalysis and Analysis on a Single Microfluidic Nanospray Chip, *Angew. Chem. Int. Ed.* **2011**, *50*, 9467–9470.

43 Okumura, M.; Yeh, L. I.; Lee, Y. T.; Vibrational Predissociation Spectroscopy of Hydrogen Cluster Ions, *J. Chem. Phys.* **1985**, *83*, 3705.

44 Brümmer, M.; Kaposta, C.; Santambrogio, G.; Asmis, K. R.; Formation and photodepletion of cluster ion–messenger atom complexes in a cold ion trap: Infrared spectroscopy of VO^+, VO_2^+, and VO_3^+, *J. Chem. Phys.* **2003**, *24*, 12700–12703.

45 Wang, X.-B.; Xing, X.-P.; Wang, L.-S.; Observation of H_2 Aggregation onto a Doubly Charged Anion in a Temperature-Controlled Ion Trap, *J. Phys. Chem. A* **2008**, *51*, 13271–13274.

46 Goebbert, D. J.; Wende, T.; Bergmann, R.; Meijer, G.; Asmis, K. R.; Messenger-Tagging Electrosprayed Ions: Vibrational Spectroscopy of Suberate Dianions, *J. Phys. Chem. A* **2009**, *20*, 5874–5880.

47 Asmis, K. R.; Brümmer, M.; Kaposta, C.; Santambrogio, G.; Helden, G. von; Meijer, G.; Rademann, K.; Wöste, L.; Mass-selected infrared photodissociation spectroscopy of $V_4O_{10}^+$, *Phys. Chem. Chem. Phys.* **2002**, *7*, 1101–1104.

48 Wang, Y.-S.; Tsai, C.-H.; Lee, Y. T.; Chang, H.-C.; Jiang, J. C.; Asvany, O.; Schlemmer, S.; Gerlich, D.; Investigations of Protonated and Deprotonated Water Clusters Using a Low-Temperature 22-Pole Ion Trap, *J. Phys. Chem. A* **2003**, *21*, 4217–4225.

49 Boyarkin, O. V.; Mercier, S. R.; Kamariotis, A.; Rizzo, T. R.; Electronic Spectroscopy of Cold, Protonated Tryptophan and Tyrosine, *J. Am. Chem. Soc.* **2006**, *9*, 2816–2817.

50 Bush, M. F.; Saykally, R. J.; Williams, E. R.; Evidence for Water Rings in the Hexahydrated Sulfate Dianion from IR Spectroscopy, *J. Am. Chem. Soc.* **2007**, *8*, 2220–2221.

51 Schulz, J.; Jašík, J.; Gray, A.; Roithová, J.; Formation of Oxazoles from Elusive Gold(I) α-Oxocarbenes: A Mechanistic Study, *Chemistry* **2016**, *28*, 9827–9834.

52 Wolke, C. T.; Fournier, J. A.; Dzugan, L. C.; Fagiani, M. R.; Odbadrakh, T. T.; Knorke, H.; Jordan, K. D.; McCoy, A. B.; Asmis, K. R.; Johnson, M. A.; Spectroscopic snapshots of the proton-transfer mechanism in water, *Science* **2016**, *6316*, 1131–1135.

53 Chiavarino, B.; Crestoni, M. E.; Fornarini, S.; Lanucara, F.; Lemaire, J.; Maître, P.; Meisenheimer Complexes Positively Characterized as Stable Intermediates in the Gas Phase, *Angew. Chem. Int. Ed.* **2007**, *12*, 1995–1998.

54 Ross, A. J.; Dreiocker, F.; Schäfer, M.; Oomens, J.; Meijer, A. J. H. M.; Pickup, B. T.; Jackson, R. F. W.; Evidence for the Role of Tetramethylethylenediamine in Aqueous Negishi Cross-Coupling: Synthesis of Nonproteinogenic Phenylalanine Derivatives on Water, *J. Org. Chem.* **2011**, *6*, 1727–1734.

55 Dunbar, R. C.; Moore, D. T.; Oomens, J.; IR spectroscopic characterization of intermediates in a gas-phase ionic reaction: The decarbonylation of Co^+(acetophenone), *Int. J. Mass. Spectrom.* **2007**, *2–3*, 182–186.

56 Wolk, A. B.; Leavitt, C. M.; Fournier, J. A.; Kamrath, M. Z.; Wijeratne, G. B.; Jackson, T. A.; Johnson, M. A.; Isolation and characterization of a peroxo manganese (III) dioxygen reaction intermediate using cryogenic ion vibrational predissociation spectroscopy, *Int. J. Mass. Spectrom.* **2013**, *354–355*, 33–38.

57 Duffy, E. M.; Marsh, B. M.; Garand, E.; Probing the Hydrogen-Bonded Water Network at the Active Site of a Water Oxidation Catalyst: $[Ru(bpy)(tpy)(H2O)]^{2+}\cdot(H_2O)_{0-4}$, *J. Phys. Chem. A* **2015**, *24*, 6326–6332.

58 Fagiani, M. R.; Knorke, H.; Esser, T. K.; Heine, N.; Wolke, C. T.; Gewinner, S.; Schöllkopf, W.; Gaigeot, M.-P.; Spezia, R.; Johnson, M. A.; Asmis, K. R.; Gas phase vibrational spectroscopy of the protonated water pentamer: the role of isomers and nuclear quantum effects, *Phys. Chem. Chem. Phys.* **2016**, *38*, 26743–26754.

59 Roithová, J.; Characterization of reaction intermediates by ion spectroscopy, *Chem. Soc. Rev.* **2012**, *2*, 547–559.

60 Elliott, B. M.; Relph, R. A.; Roscioli, J. R.; Bopp, J. C.; Gardenier, G. H.; Guasco, T. L.; Johnson, M. A.; Isolating the spectra of cluster ion isomers using Ar-"tag" -mediated IR-IR double resonance within the vibrational manifolds: Application to $NO_2^-\cdot H_2O$, *J. Chem. Phys.* **2008**, *129*, 94303.

61 Heine, N.; Fagiani, M. R.; Rossi, M.; Wende, T.; Berden, G.; Blum, V.; Asmis, K. R.; Isomer-Selective Detection of Hydrogen-Bond Vibrations in the Protonated Water Hexamer, *J. Am. Chem. Soc.* **2013**, *135*, 8266–8273.

62 Dian, B. C.; Longarte, A.; Zwier, T. S. Conformational Dynamics in a Dipeptide After Single-Mode Vibrational Excitation*Science* **2002**, *296*, 2369–2373.

63 Khanal, N.; Masellis, C.; Kamrath, M. Z.; Clemmer, D. E.; Rizzo, T. R.; Glycosaminoglycan Analysis by Cryogenic Messenger-Tagging IR Spectroscopy Combined with IMS-MS, *Anal. Chem.* **2017**, *89*, 7601–7606.

64 Seo, J.; Hoffmann, W.; Warnke, S.; Huang, X.; Gewinner, S.; Schöllkopf, W.; Bowers, M. T.; von Helden, G.; Pagel, K.; An infrared spectroscopy approach to follow β-sheet formation in peptide amyloid assemblies, *Nature Chem.* **2017**, *9*, 39–44.

For Table of Contents only